

# Photodissociation study of CH<sub>3</sub>Br in the first continuum

Theodosia Gougousi, Peter C. Samartzis, and Theofanis N. Kitsopoulos<sup>a)</sup>

*Department of Chemistry, University of Crete and Institute of Electronic Structure and Laser, Foundation for Research and Technology-Hellas, 71110 Heraklion-Crete, Greece*

(Received 20 October 1997; accepted 6 January 1998)

The photolysis of CH<sub>3</sub>Br is studied in the energy region of the A band between 4.94 and 5.76 eV using ion imaging. Velocity distributions for both the bromine-atom and methyl-radical photofragments are determined. Our results indicate that transitions to the <sup>3</sup>Q<sub>0</sub> and <sup>3</sup>Q<sub>1</sub> states dominate the absorption cross section and the partial cross section to each state is determined. The [Br\*]/[Br] branching ratio is found to be strongly dependent on the excitation energy varying between 0.6 and 1.5. Both the bromine-atom and the methyl-radical translational energy distributions suggest that the vibrational distribution in the nascent CH<sub>3</sub> is nonstatistical with appreciable excitation in the *v*<sub>2</sub> umbrella mode. The lifetime of the A band is estimated at  $\tau = 120 \pm 40$  fs. © 1998 American Institute of Physics. [S0021-9606(98)00114-7]

## I. INTRODUCTION

Methyl bromide has been the focus of much attention recently, mainly because of its ozone depletion potential.<sup>1</sup> Photodissociation via excitation to the A band (first continuum) produces ground state, Br(<sup>2</sup>P<sub>3/2</sub>), and spin-orbit excited, Br(<sup>2</sup>P<sub>1/2</sub>), bromine atoms that we label as Br and Br\*, respectively. Bromine atoms are known to be 40 times more efficient than chlorine atoms in breaking down the atmospheric ozone.<sup>2</sup> Recent studies have indicated that methyl bromide produced both by natural and anthropogenic sources is the largest reservoir of atmospheric bromide and responsible for as much as 10% of the global loss of stratospheric ozone.<sup>3</sup>

Unlike methyl iodide, which has been studied extensively,<sup>4</sup> very little work has been done on the photodissociation of CH<sub>3</sub>Br. As pointed out by previous studies,<sup>5,6</sup> the C-Br bond length (1.939 Å) in methyl bromide is substantially shorter than the C-I (2.132 Å) bond length in methyl iodide, causing the A band absorption maximum in CH<sub>3</sub>Br to shift to higher energies (~200 nm).<sup>7</sup> Excitation from the ground state can take place in three dissociative excited states, designated as <sup>3</sup>Q<sub>0</sub>, <sup>3</sup>Q<sub>1</sub>, and <sup>1</sup>Q<sub>1</sub> by Mulliken.<sup>8-10</sup> The <sup>3</sup>Q<sub>0</sub> state correlates asymptotically to CH<sub>3</sub>+Br\*, while excitations to the <sup>3</sup>Q<sub>1</sub>, and <sup>1</sup>Q<sub>1</sub> states lead to the production of CH<sub>3</sub>+Br.

Experiments performed on both sides of the absorption maximum of CH<sub>3</sub>I indicated that I\* is the major product,<sup>11</sup> and that the production of I atoms depends strongly on the extent of nonadiabatic curve crossing between the <sup>3</sup>Q<sub>0</sub> and the <sup>1</sup>Q<sub>1</sub> states. In the case of methyl bromide, however, photodissociation studies performed at 193, 222<sup>5</sup>, and 205<sup>6</sup> nm, showed that (i) the internal state distribution of CH<sub>3</sub> is hotter for the Br producing channel compared to the channel leading to the production of Br\*, and (ii) most of the CH<sub>3</sub> internal energy excitation is stored in the *v*<sub>2</sub> umbrella mode.

In this paper we present our results concerning the photodissociation of CH<sub>3</sub>Br in the wavelength range between 251 and 215 nm. Angular and translational energy distributions of the Br, Br\*, and CH<sub>3</sub> photofragments are obtained using a velocity imaging technique. The wavelength range probed covers the lower-energy portion of the absorption spectrum of methyl bromide and provides detailed information concerning the nature of the states involved in the process, their relative absorption strengths, and the [Br\*]/[Br] branching ratio.

## II. EXPERIMENT

The experimental apparatus described in detail elsewhere<sup>12</sup> is described here only briefly. A cold molecular beam is produced by expanding a gas mixture (typically 10% CH<sub>3</sub>Br in He) into the source chamber via a home-built pulsed nozzle (backing pressures  $P_0 \leq 1$  atm). The molecular beam, which is skimmed and collimated to ~0.8 mm diameter, is intersected at right angles by two counterpropagating laser beams, one used for the photolysis of CH<sub>3</sub>Br and the other for the state-selective ionization of the desired photofragment. In the case of the CH<sub>3</sub> photofragment, a *nonresonant* MPI scheme is used in order to detect all quantum states produced. To ensure that no photofragment escapes from the probe volume, a zero time delay between the two lasers is chosen. The exact wavelength of the dissociation laser is checked by resonantly ionizing either Br or Xe through a known transition, and its polarization is always maintained parallel to the detector plane. For the REMPI detection of bromine atoms, the bandwidth of the laser is found to be narrower than the velocity Doppler profile of the photofragments. Consequently, its wavelength is scanned across this profile, ensuring that all velocity components are detected with equal probability. Details about the photodissociation energies and the states involved in the REMPI detection are given in Table I.

The ions produced in the interaction region are accelerated by a suitable electric field along the axis of the time-of-

<sup>a)</sup>Electronic mail: theo@luce.iesl.forth.gr, P.O. Box 1527; telephone: ++30-81-391467; fax: ++30-81-391318.

TABLE I. Listing of the photodissociation wavelength, the measured anisotropy parameter  $\beta$ , and the intermediate states through which the (2 + 1) resonant ionization of the  $\text{Br}(^2P_{3/2})$  and  $\text{Br}^*(^2P_{1/2})$  photofragments is achieved.

Excitation wavelength (nm)	Intermediate state for Br REMPI	Intermediate state for $\text{Br}^*$ REMPI	$\beta(\text{Br})$	$\beta(\text{Br}^*)$
250.98	$^2D_{3/2}^0$	...	$0.19 \pm 0.02$	...
229.22	$^2P_{3/2}^0$	$^2P_{1/2}^0$	$0.39 \pm 0.02$	$1.94 \pm 0.05$
220.14	$^4P_{3/2}^0$	$^2P_{1/2}^0$	$-0.49 \pm 0.04$	$1.91 \pm 0.05$
215.00	$^4P_{3/2}^0$	$^2P_{1/2}^0$	$-0.11 \pm 0.02$	$1.86 \pm 0.15$

flight mass analyzer and are detected using a home-built position-sensitive ion-imaging detector. Discrimination against background ions is achieved by gating the detector and the results presented in this article are obtained by recording the  $^{81}\text{Br}^+$  ion signal. Ion images are recorded using a CCD camera and background images are obtained by tuning the ionization laser off resonance. Details about the image processing techniques and extraction of velocity distributions can be found in Ref. 12

Following the pioneering work of Eppink and Parker,<sup>13</sup> we have adopted the *velocity imaging* technique as a major modification in our experimental apparatus. The modification involves replacing the uniform extraction field assembly, which consisted of a repeller and a flat-fine-mesh grid by an electrostatic zoom lens consisting of repeller, extractor, and ground electrodes. With this arrangement, Eppink and Parker<sup>13</sup> report that ions with identical velocities produced anywhere within the interaction volume can be spatially focused to a very small “spot” on the detector ( $\sim 150 \mu\text{m}$ ). In the course of this work, because of the limited spatial resolution offered by the microsphere plates (El Mul) used in our detector, we have been able to achieve only moderate “ion-spot” sizes of  $\sim 800 \mu\text{m}$ . Even so, we find that the energy resolution of our spectrometer is improved to about 10%, from 20% when the grid is used.

### III. RESULTS

Typical data images for Br,  $\text{Br}^*$ , and  $\text{CH}_3$  produced by the photodissociation of methyl bromide are presented in Figs. 1. A first look reveals obvious differences in the angular distributions of the Br and  $\text{Br}^*$  fragments. The  $\text{Br}^*$  image has most of the intensity at the poles and very little intensity

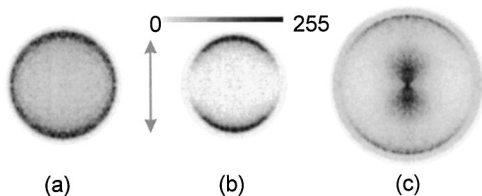


FIG. 1. (a) Image of the  $\text{Br}(^2P_{3/2})$  produced by the photodissociation of  $\text{CH}_3\text{Br}$  at 229.22 nm. (b) Image of the  $\text{Br}(^2P_{1/2})$  produced by the photodissociation of  $\text{CH}_3\text{Br}$  at 229.22 nm. (c) Image of the  $\text{CH}_3$  fragment by the photodissociation of  $\text{CH}_3\text{Br}$  at 218 nm. The arrow indicates the laser polarization direction. Intensity at the center of the  $\text{CH}_3$  image is due to the photodissociation of  $(\text{CH}_3\text{Br})_{N=2,3,4,\dots}$  clusters.

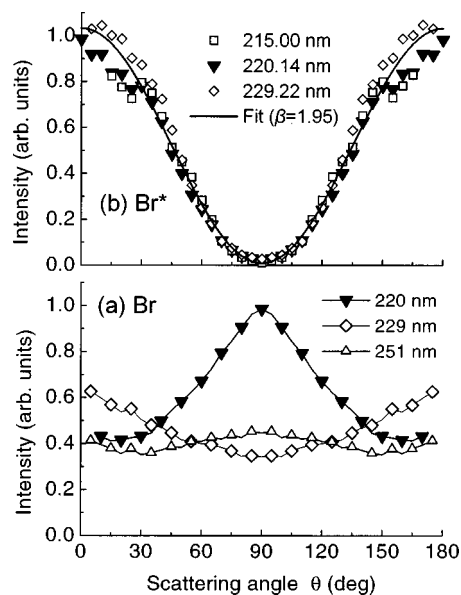


FIG. 2. (a) Angular distribution of the  $\text{Br}(^2P_{3/2})$  photofragment at a series of wavelengths. (b) Angular distribution of the  $\text{Br}(^2P_{1/2})$  photofragment obtained at a series of wavelengths.

along the equator, while the Br image is generally isotropic. In the  $\text{CH}_3$  image two distinct rings are observed that correspond to the production of Br and  $\text{Br}^*$ .

Angular distributions for Br and  $\text{Br}^*$  presented in Fig. 2 are obtained by appropriate reconstruction<sup>12</sup> of the corresponding data images. The anisotropy parameters ( $\beta$ 's) listed in Table I are determined by fitting the functional form  $I(\theta) \propto 1 + 0.5\beta(3\cos^2\theta - 1)$  to the experimental angular distributions.<sup>14,15</sup>  $\beta(\text{Br}^*)$  appears to be insensitive to the photolysis wavelength, and hence the direct measurement of the  $\text{Br}^*$  angular distribution at 251 nm was deemed redundant. On the contrary,  $\beta(\text{Br})$  displays a nonmonotonic decrease from positive to negative values as we move from the low-energy tail toward the peak of the absorption continuum.

Kinetic energy distributions (KED) that we determine by appropriate reconstruction of the  $\text{CH}_3$  images,<sup>12</sup> are shown in Fig. 3. The overlaid stick spectra indicate the calculated positions for  $\text{CH}_3$  ( $v_2, J=0$ ) and reveal several interesting trends: (a) the relative intensity of the two peaks in the  $\text{CH}_3$  KED varies as a function of wavelength; (b) both KED corresponding to the formation of the Br and  $\text{Br}^*$  peak at  $v_2^{\text{max}} > 0$ ; and (c)  $v_2^{\text{max}}(\text{Br}) > v_2^{\text{max}}(\text{Br}^*)$ .

### IV. DISCUSSION

#### A. Photofragment angular distributions and the A-band lifetime

The ground state symmetry of  $\text{CH}_3\text{Br}$  is  $A_1$  while the symmetry of the three excited states is  $E$  for the  $^3Q_1, ^1Q_1$  states and  $A_1$  for the  $^3Q_0$  state. Assuming a prompt dissociation and an axial recoil of the photofragments, then the excitations to the  $^3Q_1$  and  $^1Q_1$  states constitute perpendicular transitions, i.e., the angular distribution  $I(\theta)$  of the photofragments will follow a  $\sin^2\theta$  dependence.<sup>14,15</sup> Analogously, the transition to the  $^3Q_0$  state will be a parallel one, namely  $I(\theta) \propto \cos^2\theta$ . Hence, we expect  $\beta(\text{Br}^*) = 2.0$ , as  $\text{Br}^*$  corre-

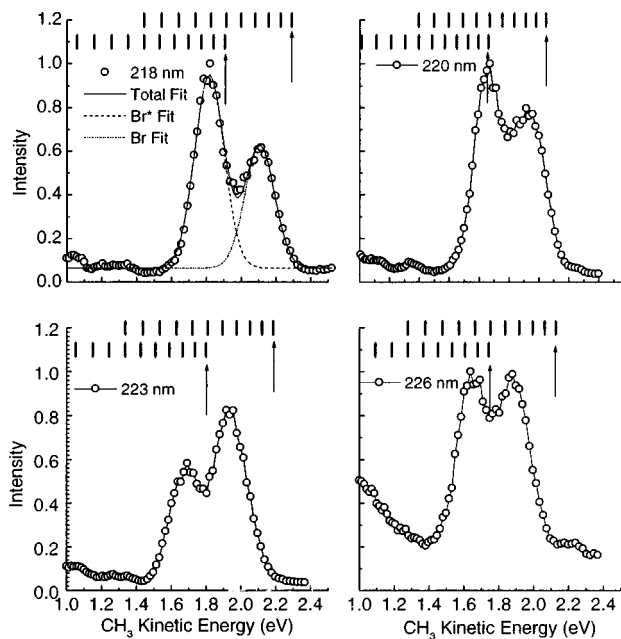


FIG. 3. Kinetic energy distributions for the  $\text{CH}_3$  photofragment. The tick marks indicate the calculated translational energies corresponding to the production of  $\text{CH}_3$  ( $\nu_2$ ,  $J=0$ ), and the arrow indicates the calculated positions for  $\text{CH}_3$  ( $\nu_2=J=0$ ) for the Br and  $\text{Br}^*$  channels, respectively. The peak appearing at  $\sim 1$  eV for the KED at 226 nm, is due to  $(\text{CH}_3\text{Br})_{N=2,3,4,\dots}$  cluster photodissociation.

lates to the  $^3Q_0$  state, and  $\beta(\text{Br}) = -1$ , as both the  $^1Q_1$  and the  $^3Q_1$  states correlate to Br. Although our observed  $\beta(\text{Br}^*) \approx 1.9$  is very close to the ideal value 2.0 predicted above, the angular distributions for Br differ substantially from the expected  $\sin^2 \theta$  behavior. These deviations can be attributed to two possible phenomena: (i) the lifetimes of the dissociative states are sufficiently long to smear out the  $\sin^2 \theta$  distribution,<sup>14,15</sup> or (ii) a sufficient amount of the  $\text{Br}^*$  produced by direct excitation is converted to Br because of nonadiabatic coupling between  $^3Q_0$  and  $^1Q_1$  states, thus adding sufficient *parallel* character to the otherwise *perpendicular* type Br angular distribution.

The first scenario assumes that the rotational period of the electronically excited  $\text{CH}_3\text{Br}$  is comparable to the time it takes for the photofragments to separate, thus changing the orientation of the dissociation axis with respect to the direction of the polarization of the photolysis laser. The coefficient  $\beta$  can be related to the lifetime  $\tau$  of the dissociative state via the relationship<sup>16</sup>

$$\beta \approx 2P_2(\cos \chi_f) \frac{1 + \omega^2 \tau^2}{1 + 4\omega^2 \tau^2}, \quad (1)$$

where  $\omega \approx (\pi kT/2I)^{1/2}$  is the angular velocity of the parent molecule,  $I$  is the moment of inertia, and  $\chi_f$  is the angle between the internuclear axis and the direction of the transition dipole for the final state. For the Br channel that involves a perpendicular transition, an extremely long lifetime  $\tau$  yields a  $\beta$  value of  $-0.25$ , and hence only the  $\beta(\text{Br})$  at 220 nm could be accounted for by the lifetime scenario. Therefore, we conclude that the semi-isotropic angular distribution of the Br photofragment is generally caused by nonadiabatic

curve crossing. For the  $\text{Br}^*$  channel, assuming a rotational temperature of  $T \approx 50$  K, we obtain  $\omega \approx 1.1 \times 10^{12} \text{ s}^{-1}$ , and setting  $\chi_f = 0^\circ$  in Eq. (1), we find that  $\tau = 120 \pm 40$  fs when  $\beta(\text{Br}^*) = 1.9 \pm 0.5$ . This value constitutes an upper lifetime limit of the A band in  $\text{CH}_3\text{Br}$  and is comparable to the results of Dzvonik *et al.*,<sup>17</sup> where a 70 fs upper lifetime limit was reported for the A band in  $\text{CH}_3\text{I}$ . From our determined lifetime setting  $\chi_f = 90^\circ$  (for the Br producing channels) in Eq. (1) we estimate that  $\beta(\text{Br}) = -0.95 \pm 0.5$ .

## B. Product state distribution

The KED for the  $\text{CH}_3$  photofragment are bimodal, each peak corresponding to the formation of Br and  $\text{Br}^*$ , respectively. As pointed out above, the  $\text{CH}_3$  internal state distribution appears to be significantly hot, for both the Br and the  $\text{Br}^*$  producing channels. As rotational structure is not observed in our data, the question we need to address concerns the partitioning of this internal energy between the rotational and vibrational degrees of freedom of the methyl radical. Both Hess *et al.*<sup>6</sup> and van Veen *et al.*<sup>5</sup> have pointed out that in order to induce large rotational excitation on  $\text{CH}_3$ , a significantly bent excited state is necessary. However, our angular distribution analysis suggests that the transition dipole moment is either parallel ( $\chi_f = 0^\circ$ ) or perpendicular ( $\chi_f = 90^\circ$ ) to the C–Br bond, leading us to believe that the  $C_{3v}$  geometry of the ground state is maintained by the excited states. In light of this argument, we conclude that most of the excitation in the  $\text{CH}_3$  must be stored as vibrational energy. In addition, given that the dissociation axis is always perpendicular (or nearly so) to the H-atom plane, it is reasonable to assume that the  $\nu_2$  umbrella mode will have the greatest probability of excitation upon photodissociation.

As in previous studies,<sup>18</sup> Fig. 3 indicates that the amount of  $\nu_2$  excitation is greater for the channel producing Br than for the channel producing  $\text{Br}^*$ . Specifically, we note that the Br KED peak at  $1\text{--}2 \nu_2$  quanta higher than the  $\text{Br}^*$  KED. Hess *et al.*<sup>6</sup> have attributed this to the difference in slopes between the potential energy surfaces, stating that the steeper  $^1Q_1$  state provides less time for the  $\text{CH}_3$  photofragment to relax. In the theoretical treatment of  $\text{CH}_3\text{I}$ , Morokuma and co-workers<sup>4,19</sup> found that the C–H bonds are situated at  $90^\circ$  angles with respect to the C–I bond in the  $^1Q_1$  state (i.e., a planar  $\text{CH}_3$  geometry), and this angle increases to about  $104^\circ$  for the  $^3Q_0$  state (i.e., a pyramidal shaped  $\text{CH}_3$ ). Their trajectory calculations showed that it is easier to excite the  $\nu_2$  mode when the  $\text{CH}_3$  is planar rather than when it is pyramidal and consequently, dissociation on the  $^3Q_0$  state generally yields cold  $\text{CH}_3$ , consistent with our observation for  $\text{CH}_3\text{Br}$ . Furthermore, Morokuma and co-workers also point out that in the case of curve crossing, the substantial change in the geometry of the methyl group from pyramidal to planar, causes a significant amount of excitation in the  $\text{CH}_3$  umbrella mode. This behavior is confirmed by our Br images by noting that the distribution of photofragments at the poles (produced by curve crossing) is noticeably wider than at the equator (direct dissociation).

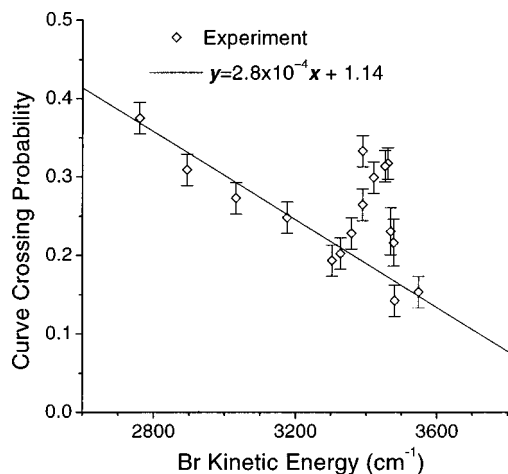


FIG. 4. Curve crossing probability  $[\text{Br}]_{\text{indirect}}/([\text{Br}^*]+[\text{Br}]_{\text{indirect}})$  as a function of Br velocity.

### C. Br\*/Br branching ratio

The amount of curve crossing is determined from the KED of  $\text{CH}_3$  obtained by considering only scattering angles in the region  $20^\circ \geq \theta \geq -20^\circ$ , i.e., only the polar part of the image, the results are plotted in Fig. 4. This procedure is justified by the conclusions presented above, mainly that the direct production of Br results in a perpendicular transition ( $\beta = -0.95$ ) and, consequently, any contribution at the poles will arise from curve crossing. In a Landau–Zener model the probability for curve crossing is proportional to  $\exp(-c/v)$  where  $c$  is a constant related to the coupling strength between the states and the slope of the potential curves, and  $v$  is the photofragment velocity at the curve crossing.<sup>20</sup> We should point out here that in a  $C_{3v}$  geometry, based on symmetry alone, the coupling between the  $^3Q_0$  ( $A_1$ ) and  $^1Q_1$  ( $E$ ) is zero ( $A_1 \otimes E = E$ ). We suspect that the nonzero coupling is caused by Jahn–Teller distortion ( $e \otimes E$ ) of the  $C_{3v}$  symmetry of the  $^1Q_1$  state via the  $\nu_6$  ( $e$  symmetry) rocking vibration.<sup>4</sup> Figure 4 clearly contradicts the Landau–Zener model as the observed propensity for curve crossing decreases with increasing Br kinetic energy and hence with  $v$  as well. Indeed, ignoring the data points between 3350 ( $\sim 220$  nm) and 3500  $\text{cm}^{-1}$  ( $\sim 224$  nm), we find that the remaining data points fit nicely to a straight line. Details about the nature of the curve crossing and the irregularity observed for excitation wavelengths between 220 and 224 nm will be discussed elsewhere.<sup>21</sup>

### D. Partial absorption cross sections

The total absorption cross section for  $\text{CH}_3\text{Br}^7$  is presented in Fig. 5. In order to extract the partial absorption cross sections  $\epsilon(^3Q_0)$ ,  $\epsilon(^3Q_1)$ , and  $\epsilon(^1Q_1)$  for the three states that comprise band A, it is necessary to know the relative amounts of Br vs  $\text{Br}^*$  produced from each state. From the KED of  $\text{CH}_3$  in Fig. 3 we determine the branching ratio  $([\text{Br}]_{\text{direct}}+[\text{Br}]_{\text{indirect}})/[\text{Br}^*] \equiv A$  by fitting the experimental distribution with two Gaussian functions, where  $[\text{Br}]_{\text{indirect}}$  and  $[\text{Br}]_{\text{direct}}$  represent the amount of Br produced

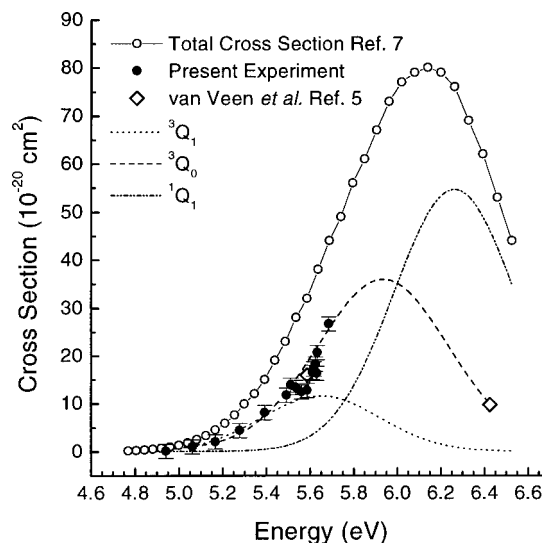


FIG. 5. Total and partial absorption cross sections of the A band for  $\text{CH}_3\text{Br}$ .

by curve crossing and by direct excitation, respectively. Hence, the relative amount of  $\text{Br}^*$  produced is given by the relationship

$$\frac{[\text{Br}^*]}{[\text{Br}^*]+[\text{Br}]_{\text{indirect}}+[\text{Br}]_{\text{direct}}} = \frac{1}{1+A}, \quad (2)$$

and the results are listed in Table II. Using Eq. (2) and the total cross section values from Fig. 5, we extract the contribution of the  $^3Q_0$  state at each wavelength studied. The results are shown in Fig. 5. Ignoring once again the data points between 220 and 224 nm, we note that a Gaussian function fits very well to our experimental points as well as the two points of van Veen *et al.*<sup>5</sup> This Gaussian function represents the absorption cross section  $[\epsilon(^3Q_0)]$  of the  $^3Q_0$  state. Subtracting  $\epsilon(^3Q_0)$  from the total cross section yields a bimodal shaped distribution that we fit with two additional Gaussian

TABLE II. Branching ratio  $[\text{Br}^*]/([\text{Br}^*]+[\text{Br}]_{\text{indirect}}+[\text{Br}]_{\text{direct}})$  for the production of  $\text{Br}^*$  and the curve crossing probability  $[\text{Br}]_{\text{indirect}}/([\text{Br}^*]+[\text{Br}]_{\text{indirect}})$ .

Excitation wavelength (nm)	$[\text{Br}]_{\text{indirect}}$	$[\text{Br}^*]$
	$[\text{Br}^*]+[\text{Br}]_{\text{indirect}}$ ( $\pm 0.02$ )	$[\text{Br}^*]+[\text{Br}]_{\text{indirect}}+[\text{Br}]_{\text{direct}}$ ( $\pm 0.05$ )
218	0.15	0.61
220	0.14	0.54
220.25	0.22	0.46
220.50	0.23	0.50
220.75	0.32	0.48
221	0.31	0.47
222	0.30	0.40
223	0.30	0.41
224	0.23	0.48
225	0.20	0.54
226	0.19	0.50
230	0.25	0.54
235	0.27	0.50
240	0.31	0.46
245	0.38	0.46

functions corresponding to  $\epsilon(^3Q_1)$  and  $\epsilon(^1Q_1)$ . Similar analysis has been reported by van Veen *et al.*<sup>5</sup> relying, however, on only two data points available at that time (193 and 222 nm). The greater number of data points obtained by the present experiment provide more stringent constraints, thus leading to a more accurate estimation of the partial cross sections. The assumption of the Gaussian shape, however, is weakened by the *anomaly* observed between 221 and 224 nm, as obviously, the Gaussian fit fails to predict the correct dynamical behavior in this energy region. Whether other such anomalous regions exist cannot be determined from the available data. Studies similar to ours, that will probe the remaining absorption spectrum of the A band, are necessary in order to completely elucidate the detailed nature of the absorption cross section.

## V. CONCLUSIONS

The photodissociation of CH<sub>3</sub>Br has been studied between 4.94–5.76 eV. For the first time separate anisotropy parameters are reported for the Br and Br\* products and an estimate for the lifetime of the A band are given. These  $\beta$ 's along with the KED of the CH<sub>3</sub> photofragment show clearly that there is an important contribution to the Br production from curve crossing between the <sup>3</sup>Q<sub>0</sub> and the <sup>1</sup>Q<sub>1</sub> state. We observe higher vibrational excitation in the  $\nu_2$  umbrella mode of the methyl radical produced by the Br rather than in the Br\* channel, which we explain in terms of the curve crossing. Finally, by analyzing the KED and photofragment angular distributions, we are able to extract the partial absorption cross sections for the <sup>3</sup>Q<sub>0</sub>, <sup>3</sup>Q<sub>1</sub>, and <sup>1</sup>Q<sub>1</sub> states of the A band.

## ACKNOWLEDGMENTS

We would like to acknowledge Professor C. Fotakis for many enlightening discussions concerning nonadiabatic pro-

cesses. Support provided by the General Secretariat for Research and Technology under the program PENED94 is gratefully acknowledged. This was conducted at the Ultraviolet Laser Facility operating at FORTH-IESL (Human Capital and Mobility, access to Large Scale Facilities EU program, Contract No. CHGE-CT92-007).

<sup>1</sup> *Scientific Assessment of Ozone Depletion: 1991* (World Meteorological Organization, Geneva, 1992), p. 4.15.

<sup>2</sup> S. C. Wofsy, M. B. McElroy, and Y. L. Yung, *Geophys. Res. Lett.* **2**, 215 (1975).

<sup>3</sup> "Methyl Bromide: Its atmospheric science, technology, and economics," United Nations Environment Program, Nairobi, Kenya, 1992.

<sup>4</sup> Y. Amamatsu, S. Yabushita, and K. Morokuma, *J. Chem. Phys.* **104**, 9784 (1996), and references therein.

<sup>5</sup> G. N. A. van Veen, T. Baller, and A. E. de Vries, *Chem. Phys.* **92**, 59 (1985).

<sup>6</sup> W. P. Hess, D. W. Chandler, and J. W. Thoman, Jr., *Chem. Phys.* **163**, 277 (1992).

<sup>7</sup> W. B. DeMore, S. P. Sander, D. M. Golden, R. F. Hampson, M. J. Kurylo, C. J. Howard, A. R. Ravishankara, C. E. Kolb, and M. J. Molina, "Chemical kinetics and photochemical data for use in stratospheric modeling," Evaluation No. 11, JPL Publication 94-26, Jet Propulsion Laboratory, Pasadena, CA, 1994.

<sup>8</sup> R. S. Mulliken, *J. Chem. Phys.* **8**, 382 (1940).

<sup>9</sup> R. S. Mulliken, *Phys. Rev.* **61**, 277 (1942).

<sup>10</sup> R. S. Mulliken and E. Teller, *Phys. Rev.* **61**, 283 (1942).

<sup>11</sup> G. N. A. van Veen, T. Baller, A. E. de Vries, and N. J. A. van Veen, *Chem. Phys.* **87**, 405 (1984).

<sup>12</sup> P. C. Samartzis, I. Sakellariou, T. Gougousi, and T. N. Kitsopoulos, *J. Chem. Phys.* **107**, 43 (1997).

<sup>13</sup> A. T. J. B. Eppink and D. H. Parker, *Rev. Sci. Instrum.* **68**, 3477 (1997).

<sup>14</sup> R. N. Zare, *Mol. Photochem.* **4**, 1 (1972).

<sup>15</sup> S. Yang and R. Bersohn, *J. Chem. Phys.* **61**, 4400 (1974).

<sup>16</sup> R. K. Sander and K. R. Wilson, *J. Chem. Phys.* **63**, 4242 (1975).

<sup>17</sup> M. Dzvoniik, S. Yang, and R. Bersohn, *J. Chem. Phys.* **61**, 4408 (1974).

<sup>18</sup> D. W. Chandler, M. H. M. Janssen, S. Stolte, R. N. Strickland, J. W. Thoman, Jr., and D. H. Parker, *J. Phys. Chem.* **94**, 4839 (1990).

<sup>19</sup> Y. Amamatsu, K. Morokuma, and S. Yabushita, *J. Chem. Phys.* **94**, 4894 (1991).

<sup>20</sup> R. D. Levine and R. B. Bernstein, *Molecular Reaction Dynamics and Chemical Reactivity* (Oxford University Press, New York, 1987), p. 377.

<sup>21</sup> P. C. Samartzis, T. Gougousi, and T. N. Kitsopoulos (in preparation).